Journal Pre-proofs

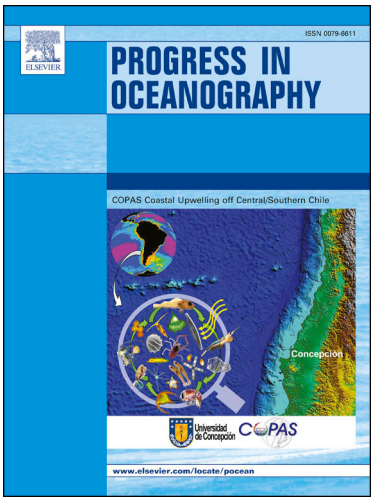

The surface salinity maximum of the South Atlantic

N. Aubone, E.D. Palma, A.R. Piola

PII: S0079-6611(20)30234-2
DOI: https://doi.org/10.1016/j.pocean.2020.102499
Reference: PROOCE 102499

To appear in: *Progress in Oceanography*

Received Date: 14 August 2020
Revised Date: 3 December 2020
Accepted Date: 9 December 2020

Please cite this article as: Aubone, N., Palma, E.D., Piola, A.R., The surface salinity maximum of the South Atlantic, *Progress in Oceanography* (2020), doi: https://doi.org/10.1016/j.pocean.2020.102499

The Surface Salinity Maximum of the South Atlantic

N. AUBONE ,[1,*] E. D. PALMA,[2] A. R. PIOLA[1,3,4]

(1) Departamento de Ciencias de la Atmósfera y los Océanos (FCEN,UBA), Capital Federal, Argentina

(2) Departamento de Física, Universidad Nacional del Sur, e Instituto Argentino de Oceanografía (CONICET), Bahía Blanca, Argentina

(3) Departamento Oceanografía, Servicio de Hidrografía Naval, Buenos Aires, Argentina

(4) Instituto Franco-Argentino sobre Estudios de Clima y sus Impactos, CONICET/CNRS, Buenos Aires, Argentina

* corresponding author, <nicolas.aubone@cima.fcen.uba.ar>

Like most other ocean basins, the maximum sea surface salinity region (MSR) in the South Atlantic shows a large displacement from the region of maximum difference between evaporation and precipitation (E-P), suggesting that ocean processes play a key role in determining the location of the MSR. We use outputs from a general circulation model (ECCO v4r3) to analyze the mixed layer salinity balance and disentangle the interaction of atmospheric forcing and oceanic processes in both regions. The MSR balance is dominated by evaporative surface fluxes and entrainment, while advection and diffusion play a secondary role. On the other hand, in the region of maximum E-P, the high surface freshwater loss is partially compensated by horizontal advection of low salinity waters, which is responsible for decreasing the salinity below that observed in the MSR. Using a particle tracking model, we find that MSR waters originate mostly from re-circulation in the Tropical South Atlantic and from the Tropical North Atlantic and Indian Oceans. After reaching the MSR, most of those waters flow southward in austral summer along the Brazil Current (1.6 Sv, 1 Sv = 10^6 m^3 s^{-1}), and northward in winter along the North Brazil Current (3.5 Sv). This seasonal variability in the fate of the salty water is modulated by the seasonal migration of the South Equatorial Current bifurcation region. Tracking of particles released at the base of the MSR mixed layer shows a subducted salt river with an estimated transport of 2.6 Sv on the 25.2 kg/m^3 neutral density surface that flows northward along the North Brazil Current and retroflects just north of the equator as part of the Equatorial Undercurrent. These high-salinity waters are a significant contributor to the upper limb of the Atlantic meridional overturning circulation and the eastern Tropical Atlantic and their variability.

Keywords : South Atlantic Ocean, Maximum Salinity Region, Salinity Budget, Mixed Layer, Salt River, South Equatorial Current Bifurcation.

Acknowledgments

This research was partially funded by project CONAE 001 from the Ministry of Science and Technology (MinCyT, Argentina), project CRN3070 from the Inter-American Institute for Global Change Research, through the US National Science Foundation grant GEO-1128040. Nicolás Aubone and Elbio D. Palma were partially supported by Agencia Nacional de Promoción Científica y Tecnológica (Argentina, grant no. PICT16-0557) and Universidad Nacional del Sur (grant no. 24F066). The ECCO data were facilitated by the ECCO Consortium group (https://ecco-group.org/home.cgi) and downloaded from ftp://ecco.jpl.nasa.gov (discontinued).

1. Introduction

Sea surface salinity is known to play an important role in the global ocean circulation and climate system variability. Subduction of high salinity surface waters in subtropical regions forms Mode Waters known as "Subtropical Underwater" [*Hanawa and Talley, 2001*] which are part of the meridional overturning circulation of the ocean, a central component of the Earth's climate system. Surface salinity is also a key indicator of surface freshwater flux patterns and variability, and the global hydrological cycle [*Schmitt, 2008; Yu, 2011*]. Recent studies show a salinity increase in high salinity regions, associated with excess evaporation, and low salinity trends in areas of excess precipitation, referred to as the "wet gets wetter" mechanism [*Durack et al., 2012; Du et al., 2019*]. Salinity is also important in determining the depth of the mixed layer and the formation of barrier layers that affect the heat exchange between the warm mixed layer waters and the colder waters below [*Lukas and Lindstrom, 1991; Sprintall and Tomczak, 1992*]. In addition, surface salinity influences the uptake of atmospheric CO_2 and O_2 [Salisbury and Jonsson, 2018; Bates and Johnson, 2020], since an increase in salinity reduces the solubility of these gases in seawater.

The combination of satellite products, atmospheric reanalysis, ocean general circulation models (OGCM) and in situ observations in the past decade, have significantly advanced the understanding of the mechanisms that maintain large-scale maximum salinity regions (MSRs) in the Tropical Atlantic [Qu et al., 20011, 2013; *Camara et al., 2015]*, the Pacific [*Hasson et al.*, 2013; *Katsura et*

al., 2013; *Gao et al.,* 2014; *Li et al.,* 2019] and the Indian Oceans [*Da-Allada et al.*, 2015; *Köhler et al.*, 2017; *Wang et al.,* 2020].

Qu et al., [2011,2013] investigated the mixed layer salinity (MLS) budget in the North Atlantic MSR using the Estimating the Circulation and Climate of the Ocean (ECCO) model. In that basin, the MSR is located poleward from the evaporation minus precipitation (E-P) maximum region and to explain the local salinity variability, ocean dynamics (advection/entrainment) is as important as atmospheric forcing (freshwater flux). The seasonal MLS cycle shows that ocean processes tend to decrease salinity throughout the year while E-P tends to increase it, since evaporation dominates the region. Analysis of the major oceanic contributors to the MLS balance shows that advection is greater during summer, when the winds are more intense, and the entrainment is greater during winter, due to increased surface cooling.

Several studies of the MLS budget in the tropical Indian Ocean reveal that the seasonal cycle is dominated by horizontal advection in the southern Arabian Sea and by the surface freshwater flux in the western Indian Ocean south of the equator, where the Intertropical Convergence Zone has a pronounced annual cycle [Da-Allada et al., 2015; Köhler et al., 2018]. With the use of satellite and Argo data, a MLS analysis was employed to explain the seasonal cycle of the MSR in the subtropical South Indian Ocean [Wang et al., 2020]. Surface salinity data provided by the Aquarius/SAC-D[(1)] satellite mission (Levine et al., 2010) revealed three distinct MSRs located south of the high E-P subtropical band, wherein the central and eastern regions sea surface salinity tendency can be explained by large seasonal changes of mixed layer depth (MLD) and surface freshwater flux. The shallow MLD (20–30 m) in austral summer amplifies the positive forcing effect of E-P and causes a sea surface salinity increase, while the deep MLD (80–120 m) in austral winter attenuates the positive E - P forcing effect and leads to a surface salinity decrease.

In the South Pacific, there is a clear shift between the location of the MSR and the E−P maxima [Hasson et al., 2013]. The study of the MLS budget with a z-coordinate OGCM (NEMO, Madec et al., 2008, at 0.25° horizontal resolution and 75 vertical levels) revealed that the seasonal cycle results primarily from a balance between the surface freshwater flux and the compensating horizontal advection and entrainment. Each of these two processes decreases the salinity by about half of the surface forcing. The North Pacific reveals two separate MSRs that roughly correspond to those of E-P maxima located to their south/southeast [Katsura et al., 2013]. The MLS variation in the eastern maximum is controlled mainly by surface freshwater flux and entrainment of fresher water through

the base of the mixed layer and is closely related to the seasonal variation of the mixed layer depth. In the western MSR, the effect of entrainment is small due to the small vertical salinity gradient across the mixed layer base, and the dominant term is E-P, that is positive throughout the year. Li et al. [2019], examine the salinity budget based on ECCO v4.3 (between 1994 and 2015) for the upper 200 m in the Pacific Ocean to explain Argo-based observations that show a salinity increase in the upper 200 m since 2005. Analyses of the salinity budget in different regions suggest that both surface freshwater and ocean advection, driven by the decadal changes of the large-scale surface winds, contribute to the salinity changes but their relative importance varies with locations.

If the sea surface salinity were determined only by surface freshwater flux, then the MSR location of all subtropical basins should match the maximum E-P region (MER hereafter). However, the above studies from other basins showed that despite the relatively complex processes determining the MLS balance, the location of the MSR lies poleward to the region of maximum freshwater loss through the sea surface. In the South Atlantic Ocean (SAO), the location of annual mean MSR (17.7°S 31°W) also lies poleward to the MER (9.5°S 15.5°W) and they are approximately 2000 km apart (Fig. 1). The large displacement between the location of the MER and MSR in the SAO strongly suggests that ocean processes play a key role in determining the location of the MSR. Camara et al. [2015] investigated the physical processes controlling the MLS seasonal budget in the Tropical Atlantic Ocean using a regional configuration of an ocean general circulation model forced by atmospheric fluxes (NEMO, Brodeau et al., 2010, at 0.25° horizontal resolution and 46 vertical levels). They found that in the SAO, around the MSR the ocean circulation and mixing acts to freshen the mixed layer against the action of evaporation. Poleward of the southern hemisphere MSR this compensation is driven through geostrophic advection and vertical diffusion of salinity in summer, and by convective entrainment during winter. In contrast, north of the salinity maximum, Ekman transport advects low salinity waters from the Intertropical Convergence Zone region that are in turn vertically offset by diffusion and evaporation. Despite being a key component of the ocean circulation [Garzoli and Matano, 2011], to the best of our knowledge, no previous studies have been focused exclusively on analyzing the SAO MSR. The aim of this work is to describe and disentangle the oceanic and atmospheric processes that drive the formation of the MSR in the South Atlantic, and its seasonal variability as well as the water mass pathways between the MSR and other oceanic regions. To this end we study the salinity budget in the mixed layer using outputs from the ECCO OGCM. To understand the importance of oceanic forcing on this budget, we compared it with the salinity balance in the MER. We also analyzed the origin and subsequent fate of the MSR waters and their possible connection with other ocean basins using a Lagrangian particle tracking model. The data and methods

are presented in section 2. In sections 3 and 4 the SAO mixed layer salinity budget and the formation and fate of MSR waters, are analyzed. The summary and conclusions are presented in section 5.

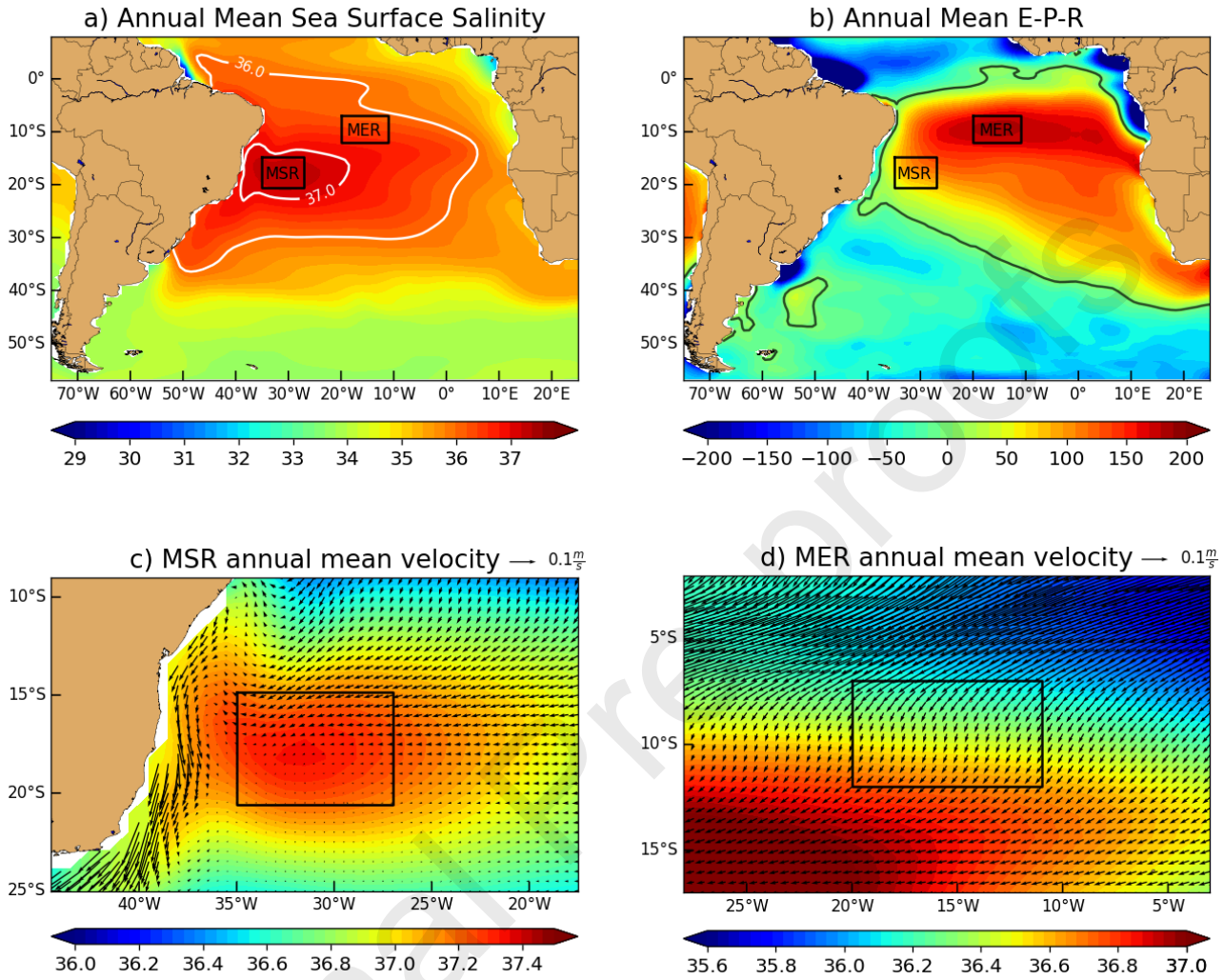

Figure 1. ECCO V4r3 annual mean 1992-2015, (a) Sea surface salinity (colors, and white contours in practical salinity unit (psu)), (b) E-P (colors, in cm/year, the zero isoline is overlaid in black), MSR (c) and MER (d) horizontal velocity, averaged in the mixed layer (black arrows) with surface salinity in colors (note the different color scales). Regions of salinity and E-P maxima are indicated with black boxes.

2. Data and Methods

2.1 Models

For this study we use monthly outputs from ECCO v4r3 [*Forget et al., 2015; Fukumori et al., 2017*] which is based on the Massachusetts Institute of Technology general circulation model [*Marshall et al., 1997*]. The estimate was produced from a least-squares fit of a free running ocean general circulation model to almost all available near-global data. It uses the adjoint method to iteratively minimize a cost function that is defined as the sum of the squared sum of weighted model-data misfits

and control adjustments. ECCO v4r3 is the final product after a series of iterations. This model version has a global coverage from January 1992 to December 2015. The grid used in v4r3 is the so-called LLC90 (Lat-Lon-Cap 90) with horizontal resolution that varies spatially from 22 km at mid latitudes to 110 km at high latitudes. The deepest ocean bottom is set to 6145 m, with the vertical grid spacing increasing from 10 m near the surface to 457 m near the ocean bottom. Velocity fields include mixing effects of mesoscale eddies that are represented using the *Gent and McWilliams* [1990] parameterization. Diffusion includes diapycnal and isopycnal components, the GGL mixed-layer turbulence closure [*Gaspar et al., 1990*], and simple convective adjustment. The ECCO mixed layer depth (MLD) data are produced on the basis of an optimal definition that employs a density-based criterion having a fixed temperature difference criterion of $\Delta T = 0.8°C$. The method is defined as the depth at the base of an isopycnal layer where the density changes by a fixed amount $\Delta\sigma = \sigma(T + \Delta T, S, P) - \sigma(T, S, P)$ from the density at a variable reference depth h_{ref}, where the pressure P is set to zero and S,T are the salinity and temperature at h_{ref} [see Kara et al., 2000 for more details]. The formation and fate of maximum salinity waters is analyzed by tracking particles with ARIANE [Blanke and Raynaud, 1997; Blanke et al., 1999]. This three-dimensional model runs on an off-line volume conservation scheme that computes particle trajectories based on output velocity fields of an OGCM. Each trajectory segment follows mass conservation and the method allows forward and backward integration of trajectories in time. The model also outputs the temperature and salinity along the trajectories of particles.

2.2 Methods

The salinity budget equation in the z^* reference frame (time invariant surface depth) was derived following Piecuch, [2017] from the salt conservation equation [Forget et al., 2015] which, averaged over the MLD can be written as :

$$\frac{\partial\langle S\rangle}{\partial t} = \left\langle \frac{1}{s^*}\left[\underbrace{S\nabla_{z^*}(s^* v) - \nabla_{z^*}(s^* S v_T)}_{horizontal advection}\right]\right\rangle + \left\langle \frac{1}{s^*}\left[\underbrace{S\frac{\partial w}{\partial z^*} - \frac{\partial (S w_T)}{\partial z^*}}_{vertical advection}\right]\right\rangle + \left\langle \underbrace{F_S}_{ice} + \underbrace{F_W}_{freshwater flux} + \underbrace{D_S}_{diffusion}\right\rangle + \underbrace{ENTR}_{entrainment} \quad (1)$$

where the angle brackets indicate a depth-average across the MLD, s^* is a scale factor ($1 + \eta/H$, η is the surface height and H the ocean depth), S is the salinity, h is the MLD, **v** and w are the horizontal and vertical components of the Eulerian velocities, $\mathbf{v_T}$ and w_T are the total velocities (Eulerian plus

bolus velocity, parameterizing the effect of unresolved eddies, [Gent and McWilliams, 1990]). The first term on the right-hand side is the depth averaged horizontal advection, and the second term is the depth averaged vertical advection. Both terms are collectively grouped into ADV, Fs is the surface salt flux due to sea ice freeze or melt, Fw is the surface freshwater flux (E-P) and **Ds** (DIFF) includes the vertical and horizontal salt diffusive mixing. The last term (ENTR) represents vertical entrainment due to mixed layer deepening/shoaling:

$$ENTR = -\frac{1}{h}\Delta S\frac{\partial h}{\partial t} \quad (2)$$

$\Delta S = \langle S \rangle - S(-h)$ is the salinity change across the base of the mixed layer. Following Gao et al. (2014) the vertical entrainment due to MLD fluctuations is computed as:

$$-\frac{1}{h}\Delta S\frac{\partial h}{\partial t} = \frac{\partial \langle S \rangle}{\partial t} - \left\langle \frac{\partial S}{\partial t} \right\rangle \quad (3)$$

that is, as the difference between the time change of the MLD averaged salinity and the average of the salinity tendency within the mixed layer.

To track MSR waters with ARIANE we feed the model with ECCO's velocity, temperature and salinity outputs and we launch 17,794 inert particles in the mixed-layer of the MSR in forward and backward mode. The particles were deployed at equally spaced locations in the horizontal domain of the MSR with a resolution of 0.2° (that is, 1271 particles on each horizontal layer). In the vertical, as the MLD is variable in space and time and to have the same number of particles for every launch, we deployed the particles within 14 equally spaced levels with a vertical resolution variable in space and time depending on the MLD at every point. To analyze the seasonal variability of the trajectories, particles were released on 60 successive months starting on January 1992 in forward mode and December 2015 in backward mode. For each launch we followed the particles during 19 years and computed the location of each particle after this period to determinate its origin or final destination. Additional experiments investigated the subduction process of MSR waters releasing particles at the base of the mixed layer.

2.3 Model Validation

Unlike most ocean reanalysis, the ECCO output variables are physically consistent with each other and with the air-sea fluxes, allowing for a full physical accounting of their temporal evolution. A prominent example of this consistency is the closure of property budgets like heat and salt [Fukumori et al., 2017], extensively used and verified in recent years [Kim et al., 2004, 2006; Qu et al., 2011, 2013; Gao et al., 2014; Thompson et al., 2016 and Cessi 2019]. To validate model data in the SAO we compare the seasonal and interannual MLS from ECCO with the Argo salinity for the period 2004–2015 [Roemmich and Gilson, 2009] (Fig. 2). At interannual time scales, the salinity is well represented in the model in both regions, with a correlation coefficient of 0.8 for MSR and 0.75 for MER (Fig. 2a). The seasonal cycle of MLS in the MSR shows good agreement in phase and amplitude of both time series, but displays a phase difference between April and August in the MER (Fig. 2b). Additionally, the model sea surface salinity is in good agreement with monthly salinity data provided by the SMOS[(2)] satellite mission between May 2010 and December 2015 (Fig. S1). Similarly, ECCO's net surface freshwater fluxes compare well with the monthly mean freshwater flux from OAFlux [Yu, 2007] and GPCP [Adler et al., 2016] during the period 1992-2015 (Fig. S2). It is important to note that ECCO is constrained by Argo observations, therefore the model salinities are not fully independent from Argo data. These comparisons show that the seasonal and interannual variability of the model's MLS in the MSR and MER is consistent with surface and subsurface observations; we therefore conclude that ECCO can be used to study the salinity budget in these regions.

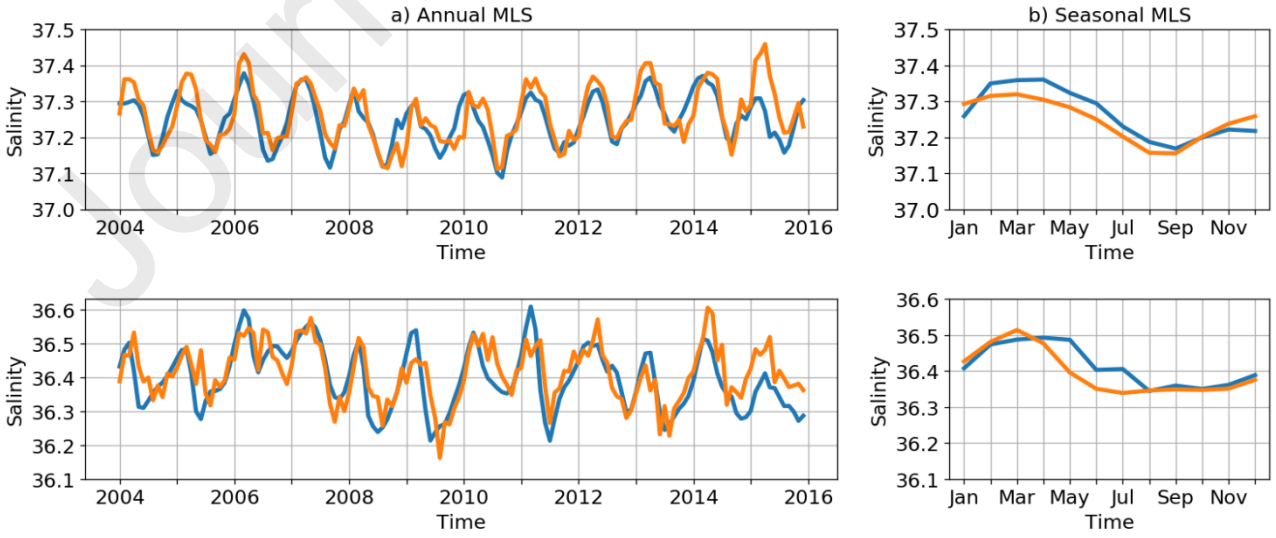

Figure 2. a) interannual mixed layer salinity and b) monthly mean seasonal salinity in the mixed layer (both in practical salinity, psu) from ECCO (orange) and ARGO (blue) in the MSR (top) and MER (bottom). Note that the salinity scale is different for the top and bottom panels.

3. Mixed Layer Salinity Balance

The MSR and MER present a seasonal salinity cycle in the mixed layer with higher values in late summer and minimum values in late winter (Fig. 2, right panels). To understand the nature of the basin-wide salinity variability we computed the dominant terms (higher absolute annual mean value) of the right-hand side terms of Eq. (1). The budget is closed by the tendency term (left-hand side of Eq. (1)) to O(10^{-5}). The spatial distribution of the dominant terms of the MLS balance reveals the dominant processes in each part of the basin (Fig. 3). F_w dominates the central tropical South Atlantic where the MSR is located, the core of the subtropical gyre (36°W 29°S) and a zonal band north of the equator, in concordance with evaporation and precipitation maxima shown in Fig. 1b. Salinity advection by ocean currents is predominant in the intertropical SAO north of 10°S, where relatively strong southwestward currents of the Central South Equatorial Current (CSEC) intersect the MER and also around the edge of the subtropical gyre and the Brazil/Malvinas Confluence. Entrainment is dominant along the southern edges of the subtropical gyre and the southern portion of the Malvinas Current. Diffusion is larger along a narrow equatorial band, close to river discharge regions (Amazon, Congo, de la Plata and Niger) and south of 40°S.

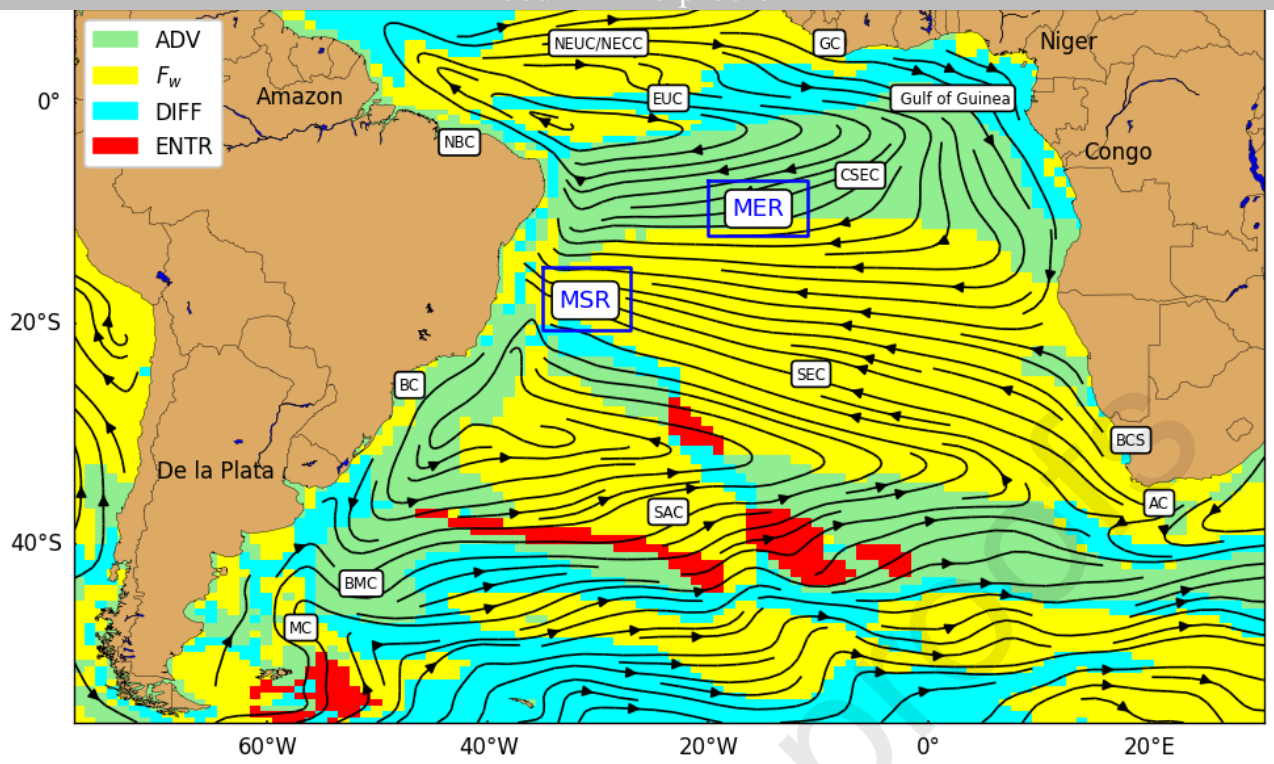

Figure 3. Dominant processes in the mixed layer salinity budget in the South Atlantic Ocean: advection (light-green), surface freshwater flux (yellow), diffusion (cyan) and entrainment (red). Advection and diffusion components include the sum of their respective horizontal and vertical terms. The MSR and MER are indicated by blue boxes. Most important rivers are marked over the continents. Annual-mean streamlines computed from ECCO v4r3 depth-average velocity field (upper 150 m) are shown in black and the main currents indicated as follows: NEUC (North-Equatorial Undercurrent), NECC (North-Equatorial Counter-current), EUC (Equatorial Undercurrent), GC (Guinea Current), NBC (North Brazil Current), CSEC (Central South Equatorial Current), SEC (South Equatorial Current), BC (Brazil Current), BCS (Benguela Current System), SAC (South Atlantic Current), AC (Agulhas Current), MC (Malvinas Current) and BMC (Brazil/Malvinas Confluence).

In the MSR, the annual cycle of MLS is dominated by the F_w and entrainment processes, with amplitudes higher than 0.05 psu/month (Fig. 4a). The F_w forcing acts to increase the MLS yearlong in response to the higher evaporation rate that prevails in the subtropical region. Given that the waters below the mixed layer are fresher, the entrainment variability with positive and negative values is explained by the seasonal displacement of the mixed layer depth. Since by definition the MSR is surrounded by low salinity waters, turbulent mixing acts to decrease the MLS. The freshening effect caused by horizontal advection of low salinity waters from the north and east plays a secondary role in this region. The seasonal cycle shows that the MLS tendency (Fig. 4b, black curve) is modulated by F_w during summer and by entrainment the rest of the year, which reaches its negative maximum during winter when the surface cooling deepens the mixed layer down to ~140 m, and maximum values in September after its upward retreat to ~ 40 m. The minor role of diffusion and advection is to freshen the MLS yearlong and is somewhat more important in summer when the impact of entrainment is negligible.

In the MER the MLS balance shows a positive F_w forcing (net freshwater loss from the ocean) throughout the years but with a long-term mean that nearly doubles the freshwater loss in the MSR (Fig. 4c). This salinification of the mixed layer by strong evaporation is largely compensated by a large inflow of fresher waters (ADV ~ -0.3 psu/month in several years). In fact, the advection effect (blue line in Fig. 4c) exceeds the impact of F_w (red line in Fig. 4c), and the salinity budget is closed by small positive (0.02-0.03 psu/mo) contributions of entrainment (green) and diffusion (orange). The seasonal cycle in the MER shows that the MLS tendency is negative during autumn, dominated by strong negative advection despite the F_W maximum, and positive during summer, when advection reaches its minimum (Fig. 4d). The enhanced advection in autumn is associated with intense, cross-isohaline wind driven currents. The horizontal advection contribution, an order of magnitude larger than in the MSR, is mediated by the CSEC that carries low salinity surface waters from tropical latitudes to the MER (Fig. 1d).

These results reveal that at seasonal time scales, both regions have a strong influence of ocean dynamics in shaping the MLS variability. The role played by each forcing setting this salinity balance is consistent with previous results in the SAO evaporative region [Camara et al., 2015].

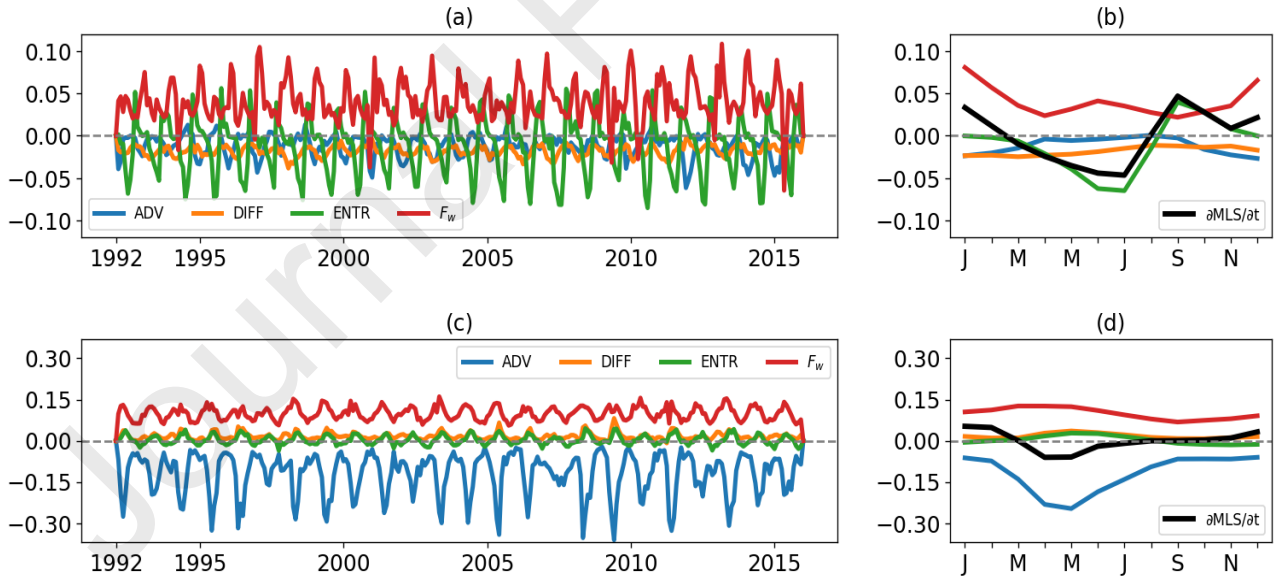

Figure 4. Annual and seasonal salinity balance (psu/month) in the two regions of study. The upper panel shows the a) annual and b) seasonal terms of salinity balance equation for the MSR and the bottom panel the c) annual and d) seasonal terms for the MER. Advection (blue), Diffusion (orange), Entrainment (green) and F_w (red). Advection and diffusion components include the sum of their respective horizontal and vertical terms. The black curve in the right panels indicates the tendency term. It was not included in the left panels for clarity. Note that the salinity scale is different for the top and bottom panels.

4. Origin and Fate of MSR waters

In this section we explore the origin and subsequent fate of MSR waters employing particle tracking experiments integrated in backward and forward mode respectively. Particles are deployed equally spaced in a control volume encompassing the MSR region and within the depth of the mixed layer. To investigate the effects of the seasonal and interannual variability of the circulation these particles are released at the beginning of every month and followed during 19 years. Figures 5 and 6 and Suppl. Figs. S3 and S4 show two examples of particle trajectories projected on a horizontal plane and released in September 2011 (backward) and June 1992 (forward). After year 10, both backward and forward experiments show that the particles are either out of the SAO domain or recirculate within the SAO subtropical or tropical gyres (not shown). Results concerning the seasonal variability of the path of MSR waters are included in Table 1. The backward experiment (Fig. 5 and Fig. S3) shows that ten years before reaching the MSR mixed layer, low-salinity (< 35 psu) subsurface particles enter the SAO from the Indian Ocean through the Agulhas Current (AC) leakage and Benguela Current system (BCS) and later flow northwestward following the South Equatorial Current (SEC). North of the MSR other low salinity particles flow northward as part of the North Brazil Current (NBC) and subsequently veer eastward through the Equatorial Undercurrent (EUC) and the North Equatorial Undercurrent (NEUC) and reach the Gulf of Guinea. In addition, surface particles from the Tropical North Atlantic enter the SAO through its eastern boundary, following the African coast along the path of the Guinea Current. Eight years before reaching the MSR, low salinity particles from the Antarctic Circumpolar Current (ACC) enter the SAO through the Malvinas Current and the adjacent continental shelf, while other surface particles with higher salinity (>36 psu) flow southward along the western boundary following the Brazil Current (BC) and the southern limb of the subtropical gyre to subsequently reach the MSR driven by the SEC. By the year -6 particles from the Indian Ocean are located mostly in the BCS and those from the subtropical gyre gain salinity as they approach the MSR. Some subsurface particles flow towards the Indian Ocean advected by the South Atlantic Current (SAC). Four and two years before reaching the MSR, particles circulating in the tropical region that concentrate in the Gulf of Guinea are upwelled and gain salinity as they move southwestward to the MSR following the CSEC. After ten years, all particles arrived to the MSR. At the end of the 19 year backward run about 42% of the particles recirculate in the SAO, 31% enter from the Tropical North Atlantic, 26% from the Indian Ocean (Agulhas leakage) and only 1% from the Pacific (ACC) (Table 1). Analysis of the seasonal results revealed a balance between the particles arriving from the SAO and Tropical North Atlantic in austral winter (JAS) and summer (DJF), with

a ~13% difference between the two seasons. Percentage of particles from the Indian and Pacific Oceans seem stable yearlong.

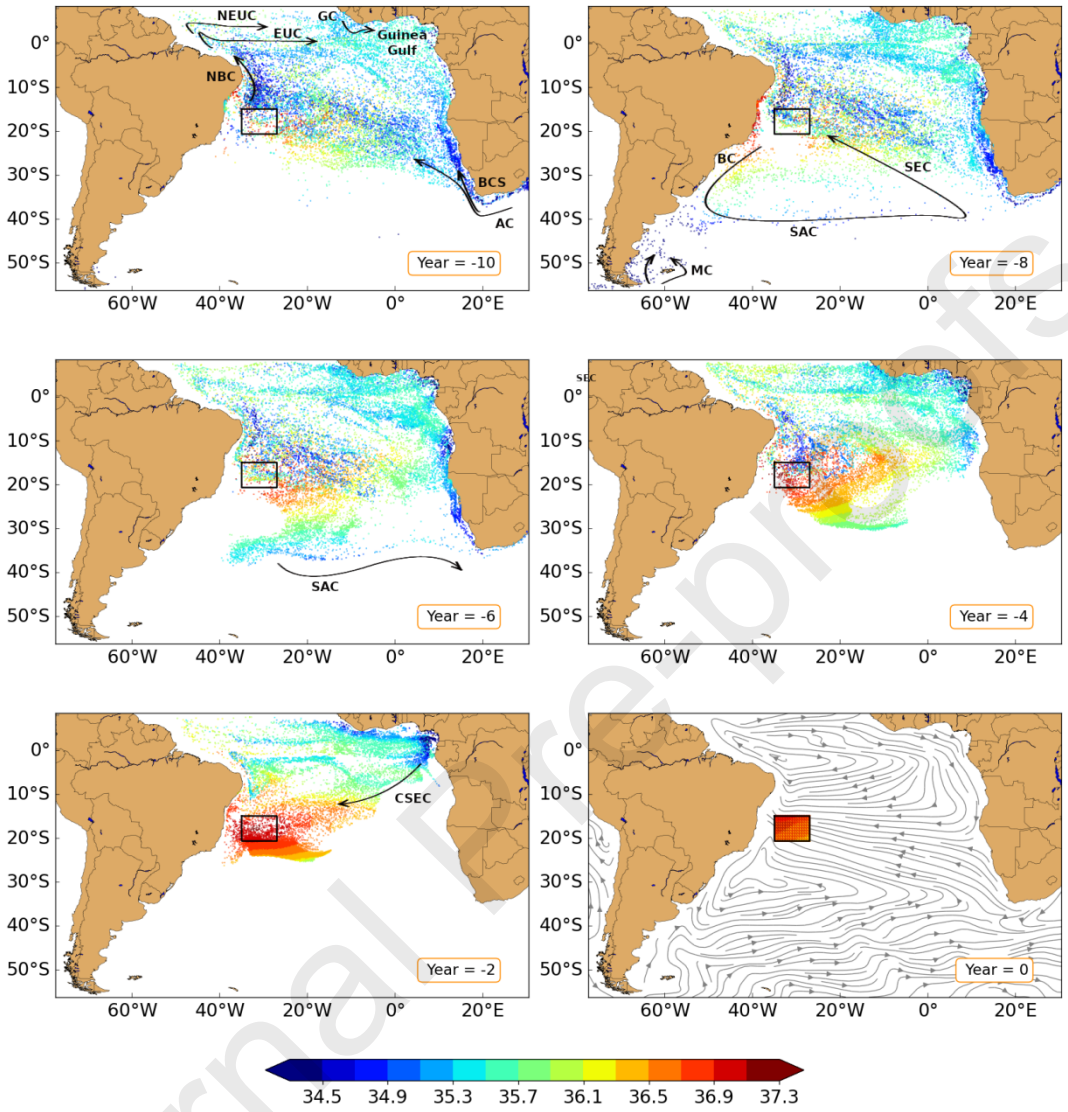

Figure 5. Sequence of 10 years of particles advected backward in time until they reach the mixed layer MSR in September 2011. Colors indicate particle salinity (psu). Black arrows in each panel schematically illustrate the upper-layer currents of the SAO, also shown in grey (year 0) are the annual-mean surface (upper 20 m) streamlines. The black box indicates the MSR.

	S. Atlantic	Tropical N. Atlantic	Indian	Pacific
Origin				
Annual	42	31	26	1
Summer	38	36	25	1
Winter	49.7	22	27	1.3
Destination				
Annual	53	46.7	0.3	-
Summer	58.7	41	0.3	-
Winter	46.4	53.3	0.3	-

Table 1. Origin (backward experiment) and destination (forward experiment) percentages (%) of particles in the MSR derived from distinct regions for the 19 years run. Annual-mean, summer and winter statistics are shown.

The forward experiment (Fig. 6 and Fig. S4) shows that particles released in the MSR flow westward until they reach the east coast of South America (the SEC bifurcation region) and consequently, either turn northward following the path of the NBC or southward advected by the BC. Two years after leaving the MSR, the northward flowing particles of the upper mixed layer lose salinity and cross the equator into the Tropical North Atlantic. Particles initially at the bottom of the mixed layer turn eastward following the EUC and NEUC. These subsurface particles are driven by subduction of mixed layer waters into the stratified thermocline. Most of the particles that follow the BC path flow southward until the current separates from the shelf break and turns eastward to the open ocean at the Brazil/Malvinas Confluence (~37°S). Subsequently, they are advected by the SAC with a marked decrease in salinity due to isopycnal mixing with Subantarctic waters along the Subtropical Front (Piola and Gordon, 1989) and to less extent by winter convection. At year 4, subsurface particles have reached the coast of Africa near the equator and after being upwelled proceed westward, back to the MSR. By year 6 and 8 all the particles have left the MSR. Particles that return to the MSR get caught again in the SEC bifurcation and the cycle, mainly in the subtropical gyre, is repeated. A small fraction of the fresher waters carried by the SAC escape to the Indian Ocean. Ten years after departing from the MSR the majority of the particles concentrate within the subtropical gyre and few particles remain north of this region. At the end of the experiment, 53% of the particles launched remain in the SAO (~59% in austral summer and ~46% in winter) while ~47% (41% in summer and ~53% in winter)

flow beyond 10°N into the Tropical North Atlantic, mainly along the western boundary. Only a minor fraction of the particles (0.3%) reach the Indian Ocean (Table 1). To investigate the cause of this seasonal variability we compute the number of particles flowing northward (NBC) and southward (BC) after leaving the MSR. In austral summer nearly 60% of the particles released in the MSR flow southward following the BC path and the remaining particles turn northward along the NBC. The fate of southward and northward flowing particles reverses in winter, with 60% of the particles following the NBC. This seasonal variability of the path of water leaving the MSR is due to the latitudinal migration of the SEC bifurcation. Previous studies based on numerical models have shown that the SEC bifurcation latitude reaches its southernmost position in July (~17°S in the top 200 m) and its northernmost position in November (~13°S in the top 200 m). Model results also showed that most of the meridional fluctuation of the bifurcation at seasonal time scales is associated with changes in the local wind stress curl due to the annual north–south excursion of the Intertropical Convergence Zone [Rodrigues et al., 2006].

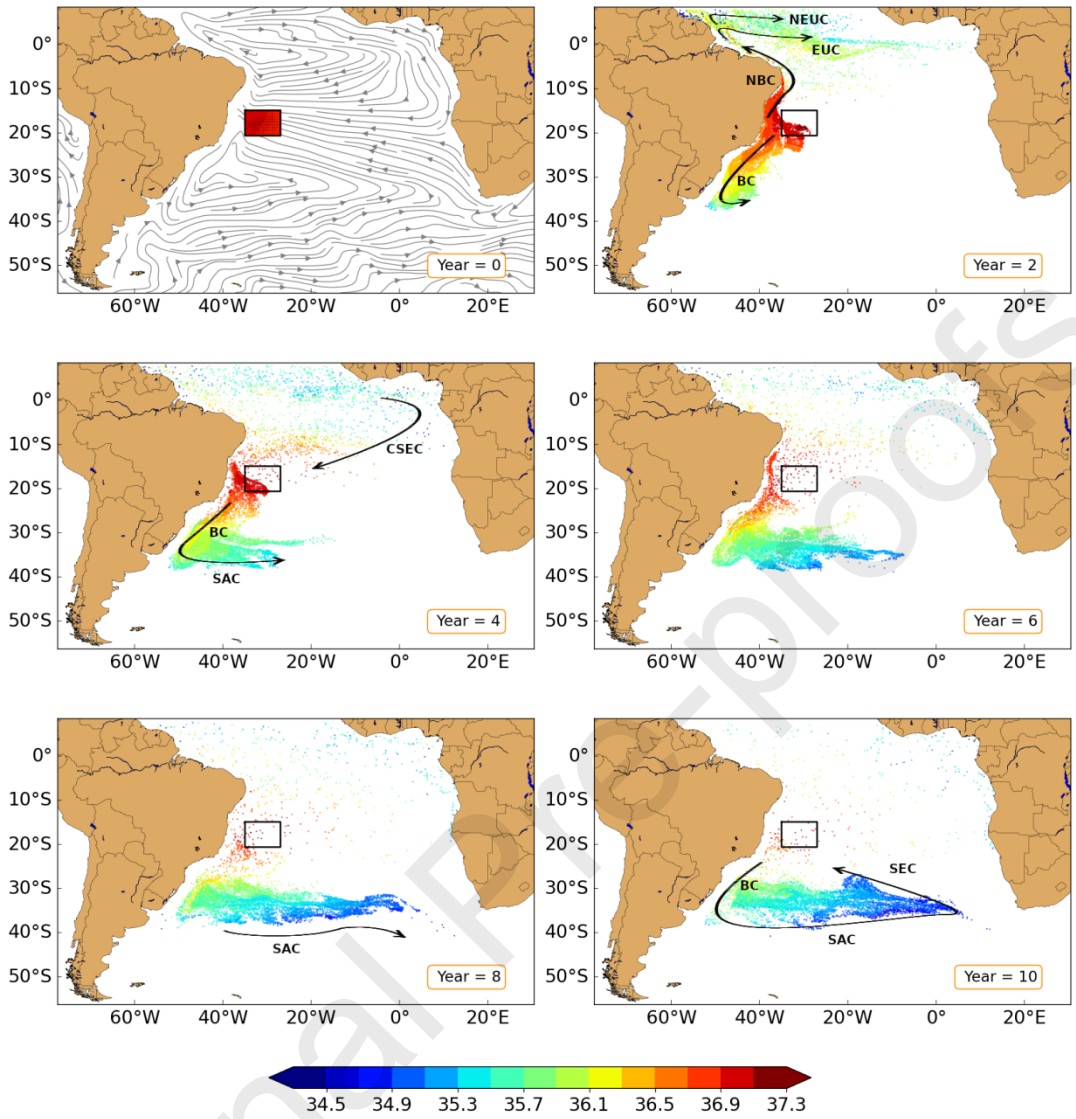

Figure 6. Sequence of 10 years advected particles forward in time leaving the MSR in June 1992. The color palette shows the salinity (psu) along particles trajectory. Black arrows illustrate the principal currents of the SAO and in grey (year 0) are the annual-mean surface (upper 20 m) streamlines. The black box indicates the MSR.

To determine to what extent the seasonal migrations of the SEC bifurcation can explain the changes in the fate of particles released in the MSR we computed the bifurcation latitude using the climatological velocity fields from ECCO. The bifurcation latitude was computed as the location where the mean meridional velocity of the two cells closest to the western boundary shift from southward to northward direction. Model results show a SEC northernmost bifurcation latitude near 11°S in late spring (November-December) and southernmost in 15.8°S for early winter (May-July) (Fig. 7). When the bifurcation is in the northernmost latitude, most of the water leaving the MSR first

flows northwestward and then describes a sharp anticyclonic turn and proceeds southward following the BC (Fig. 7a). In late spring, as the bifurcation shifts southward matching the northern boundary of the MSR near 15.8°C, the majority of the particles have a tendency to flow northward following the NBC (Fig. 7b). To quantify what fraction of the NBC and BC transport originates in the MSR we construct two cross-sections at 10°S and 22°S based on the spatial distribution of the particles (not shown). For the BC the zonal section extends from the coast to 38°W and from the surface to 50 m depth. For the NBC, the cross-section extends from the coast to 33.5°W and from the surface to 182 m. The different vertical dimensions take into account the different vertical extent of particles derived from the MSR in each region.

In the BC section, we found an annual-mean southward volume transport of 1.6 ± 0.4 Sv (1 Sv = 10^6 m^3 s^{-1}) (Fig. 7c). Salinity across this section seems weakly modulated by the volume transport with a correlation coefficient of 0.3 (two months lag, significantly different from zero at 99% confidence). In the NBC section, the volume transport also shows a seasonal cycle but a higher annual mean (3.5 ± 1.1 Sv) (Fig. 7d). In this section salinity is significantly correlated with the transport cycle (0.6) and highlights the importance of the SEC bifurcation in advecting salty waters northward. The Atlantic Meridional Overturning Circulation (AMOC) is commonly defined as the zonally and vertically integrated northward volume transport in the Atlantic; and is therefore defined as a function of latitude and depth. The AMOC strength as a function of latitude is typically defined as the maximum transport over depth [Buckley and Marshall, 2016]. Using the ECCO velocity field, the computed annual mean AMOC intensity at 10°S was 13.7 ± 3 Sv. This value is comparable although lower than the 16.2 ± 3 Sv computed at 11°S employing inverse techniques with hydrographic and current-meter data [Lumpkin and Speer, 2007]. This underestimate of the AMOC strength (which is similar at other latitudes) in assimilation models like ECCO seems to be related to spurious mixing in overflow regions that leads to a relatively weak Deep Western Boundary Current and overturning cell [Buckley and Marshall, 2016]. Given the high correlation (r = 0.7) among the surface expression of the NBC transport with the AMOC intensity (not shown) and with the MLS (r = 0.6) and the results of the forward Lagrangian experiment we conclude that ~25% (13.7 Sv x 0.25 ~ 3.5 Sv) of the northward flowing upper limb of the AMOC at 10°S is composed by waters derived from the MSR region in the South Atlantic. Nearly 30 % of the particles flowing northward in the NBC flow directly through 10°N into the Tropical North Atlantic, while the remaining particles cross that latitude after recirculating through the Tropical South Atlantic.

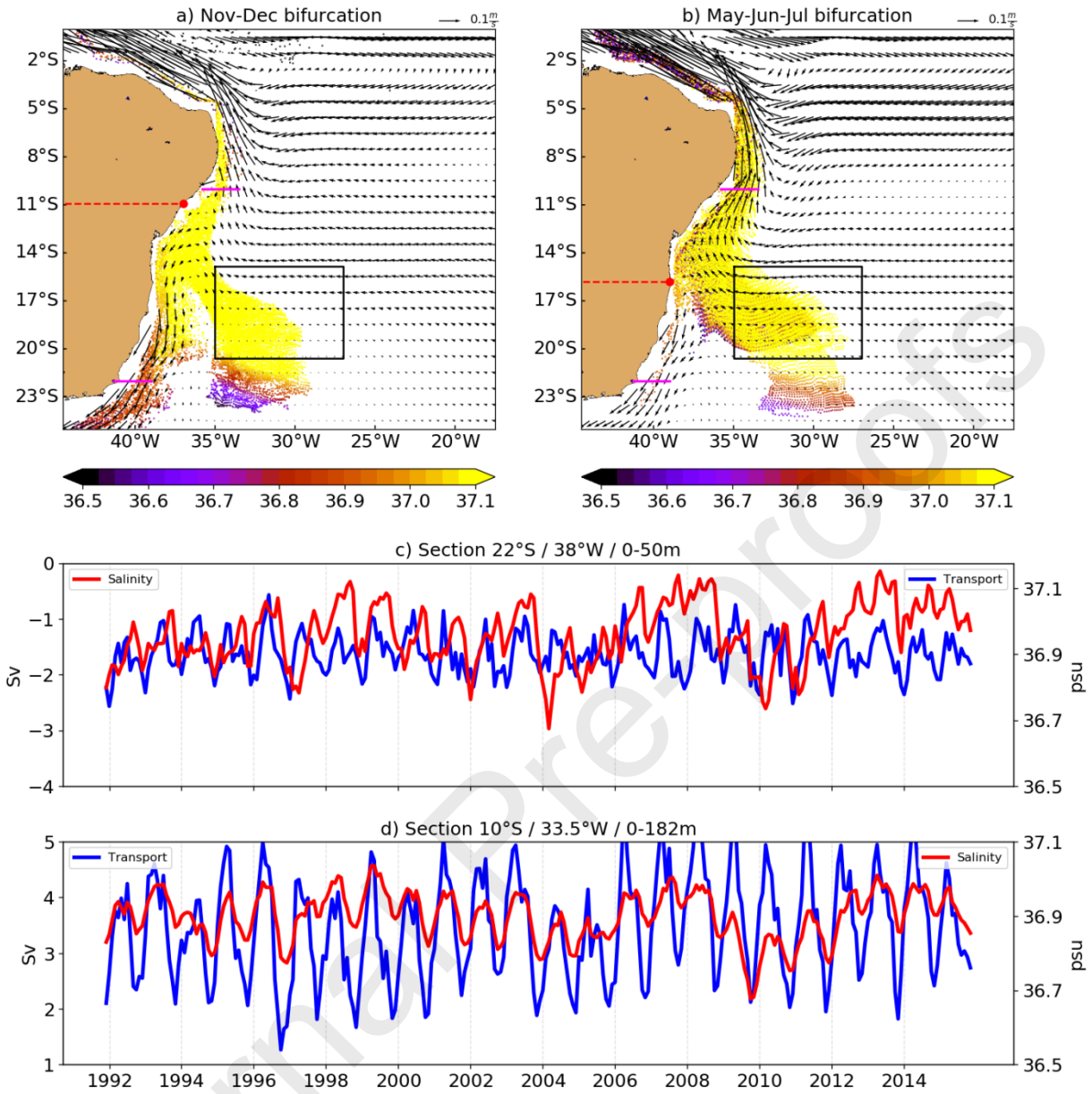

Figure 7. Upper 200 m mean current velocities (black arrows) for climatological a) late spring (ND) and b) early winter (MJJ). The red dot indicates the latitude of the SEC bifurcation and the black box the MSR region. Also shown are the launched particles locations and their salinity after leaving the MSR for a summer (a) and winter (b) experiment. The bottom panels show the annual mean volume transport (Sv) and salinity (psu) for two zonal sections (magenta lines) in c) 22°S delimited by coast and 38°W, d) 10°S delimited by the coast and 33.5°W.

Finally, we analyze in detail the subducted particles from the bottom of the mixed layer that leave the MSR and flow northward following the NBC as described above (see Fig. 7b). Waters at the base of relatively deep mixed layers located close to sharp MLD fronts (where the mixed layer depth changes sharply in a narrow band) tend to irreversibly subduct below the thermocline/halocline. To quantify the annual subduction rate we use a simplified Lagrangian method [Woods, 1985; Qiu and Huang, 1995] that can be written as :

$$V = \frac{1}{T}[(D_f - D_0) - (MLD_f - MLD_0)] \quad (4)$$

where V> 0 means that the fluid is being transferred into the thermocline, T is the time from September (when the MLD reaches its maximum thickness) to September of the following year, and D_f, D_o are the depths of the particles at the end and the beginning of the path. MLD_f and MLD_0 are the depth of the mixed layer in September of the first and second year respectively. The first term in Eq. (4) represents the contribution of vertical motion, mostly due to Ekman pumping, and it is the vertical displacement of a particle in one year. The second term represents the lateral induction and is the vertical displacement of the MLD in one year. The units of Eq. (4) are m/yr, so the multiplication of V with the MSR horizontal area gives the subducted volume transport. To compute the annual mean subduction rate of the MSR we launch 1,271 particles every September (a particle every ~0.2°) at the base of the mixed layer and follow them during one year using ARIANE with ECCO velocity outputs. The subduction process occurs in late winter, in regions where the MLD fronts intersect the outcropping isopycnals, and it is enhanced in maximum salinity regions and subtropical gyres [Williams, 1991; Marshall et al., 1993, Kubokawa, 1999]. To trace the salty water subducted in the SAO, we choose the September climatological neutral density surface that outcrops in the MSR and intersects the MLD front (γ^n = 25.2 kg/m^3). Fig. 8 shows the salinity and velocity fields projected onto this neutral density surface. Water initially at the bottom of the MSR mixed layer is subducted to the permanent pycnocline and advected towards the coast of Brazil and then northward by subsurface currents along the NBC. Following Schmitt and Blair [2015] this subsurface tongue of salty waters (> 36.5 psu) is referred to as 'salt river'. After its retroflection near the equator these waters become part of the EUC and gradually dilute (<36 psu) in the equatorial region until they reach the Gulf of Guinea. The salinity decrease in the EUC was first described by Metcalf et al. [1962] and later confirmed by Gouriou and Reverdin [1992]. The main physical mechanism behind the freshening of the EUC has been attributed to shear-induced vertical mixing in the upper edge and convective downwelling in the bottom edge [Wang, 2005; Claret et al., 2012]. The erosion of the salinity maximum of the EUC is also a qualitative indicator of the intense vertical mixing in equatorial regions and can be used to assess nutrient enrichment and primary production at the equator and Gulf of Guinea [Voituriez and Herbland, 1979; Christian and Murtugudde, 2003]. The averaged annual subduction rate (Eq. 4) in the MSR is 2.6 Sv were 2 Sv (78%) correspond to lateral induction and 0.6 Sv (22%) to vertical pumping. This difference is explained by a marked decrease (~71 m) in the September MLD along the northward path of the particles as they follow the NBC, against a main

vertical displacement of the particles (vertical pumping) of ~20 m. This is in contrast with the subduction estimated in the North Atlantic maximum salinity region, where 72% of the annual subduction rate is generated by vertical pumping and only 28% by lateral induction [Qu et al., 2013]. These differences arise from the fact that the North Atlantic MSR lies in the central subtropical gyre, where vertical Ekman pumping is enhanced, and also because its salty waters are advected westward in a one-year timescale, resulting in a minimum MLD variation that is associated with low lateral induction. In contrast, the South Atlantic MSR is located on the western boundary of the basin and the waters are rapidly advected equatorward where the prominent MLD decrease induces substantial lateral induction.

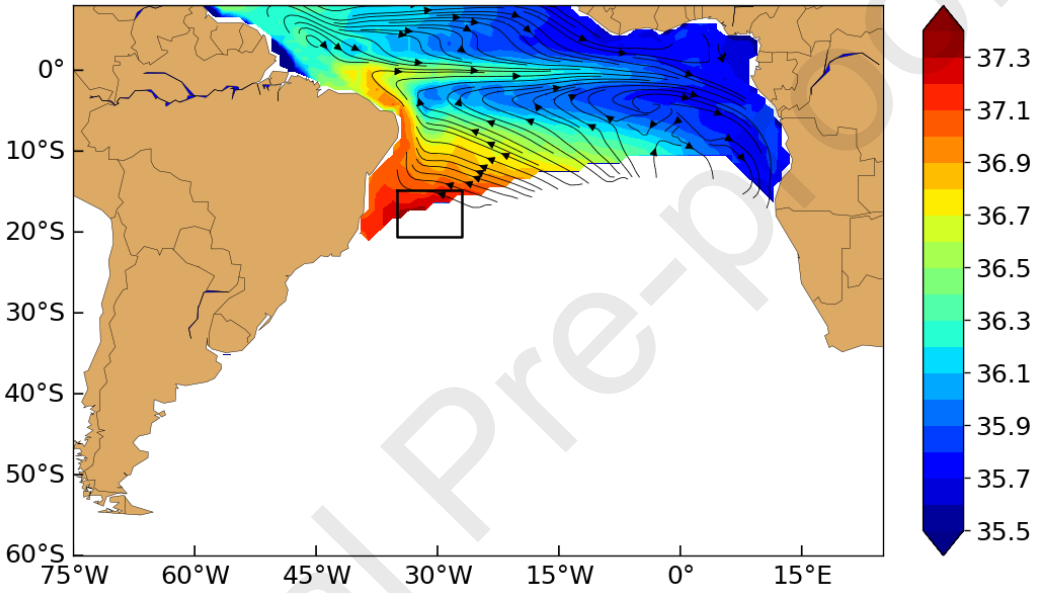

Figure 8. September climatological distribution of salinity (psu) over the $\gamma^n = 25.2$ kg/m^3 neutral density surface. Blanked areas indicate surface isopycnal outcrop. Black arrows represent the stream flow over the isopycnal layer. The MSR region is indicated by the black box.

5. Summary and conclusions

The ECCO model was used to study the mixed layer salinity balance in the maximum salinity region (MSR) in the South Atlantic Ocean. The MSR in the South Atlantic is about 2000 km away from the region of maximum freshwater loss through the sea surface, suggesting that ocean dynamics play a key role in shaping the salinity distribution. The MLS balance shows that the MSR is dominated by a balance between net freshwater fluxes through the sea surface and entrainment, with amplitudes larger than 0.05 psu/month and with horizontal and vertical advection and diffusion playing a secondary role in freshening the mixed layer. While the surface freshwater flux acts to increase the

MLS yearlong, entrainment oscillates between positive and negative values due to seasonal displacements of the mixed layer depth.

In the maximum evaporation minus precipitation region (MER), although annual mean net freshwater flux through the sea surface is twice as large as over the MSR, the salinity balance is dominated by strong freshening promoted by horizontal advection. The advective contribution to the mixed layer salinity budget (~0.25 psu/month in May) is an order of magnitude larger than over the MSR. Diffusion and entrainment play a relatively minor role in increasing the MER salinity in austral autumn. These results highlight the importance of horizontal advection in transferring relatively low salinity waters from the near-equatorial region and the Gulf of Guinea into the MER, and explain the large displacement of the maximum salinity region from the region of maximum freshwater loss through the sea surface.

Particle tracking experiments showed that MSR waters originate from the Tropical North Atlantic Ocean (31%) flowing southward along the path of the Guinea Current and from the Indian Ocean (26%) that flow northward into the Benguela Current system. The remaining waters (42%) recirculate within the South Atlantic. When reaching the African coast, the tropical waters upwell to the surface and eventually reach the MSR following the CSEC. Salty waters leaving the MSR are advected by the westward flowing SEC. As the SEC bifurcation migrates southward during austral early winter (15.8°S), more MSR waters flow northward following the NBC. In contrast, during late spring, the SEC bifurcation reaches its northernmost position (11°S) and a majority of salty MSR water flows southward following the BC and join the Subtropical Gyre. After ten years, almost all particles north of the MSR flow into the Tropical North Atlantic (47%) while southward particles remain recirculating in the Subtropical Gyre (53%). Only a small fraction (0.3%) of the particles flow into the Indian Ocean. The computed annual mean volume transport of MSR waters into the BC and NBC was ~1.6 Sv and 3.5 Sv respectively. The salty waters of the NBC represent nearly 25% of the model upper limb of the AMOC northward transport through 10°S and the Lagrangian experiments show that these waters flow into the North Atlantic either directly along the western boundary (30%) or after recirculating through the Tropical South Atlantic (70%). Waters subducted in the MSR form a northward flowing salt river on the 25.2 kg/m^3 neutral density surface, exporting salty waters (>36.5 psu) to the NBC and the eastern Tropical Atlantic following the path of the EUC. The estimated annual-mean subduction rate in the MSR is 2.6 Sv, mostly due to lateral induction (78%) and to a lesser extent due to vertical pumping (22%). This result shows that almost all the water advected northward from the MSR subducts due to its high salinity. These waters are a significant contributor to the AMOC and the eastern Tropical Atlantic and their variability.

[1] Aquarius L3 Sea surface salinity monthly composite. These data were obtained from the Physical Oceanography Distributed Active Archive Center (PODAAC) of NASA, JPL Laboratory, and CALTECH (USA).
https://podaac.jpl.nasa.gov/dataset/AQUARIUS_L3_SSS_SMI_ANNUAL_V5

[2] SMOS L3 Sea surface salinity monthly Composite. These data were obtained from the Ocean Salinity Expertise Center (CECOS) of the CNES- IFREMER Centre Aval de Traitemenent des Donnees SMOS (CATDS), at IFREMER, Plouzane (France)).
http://www.salinityremotesensing.ifremer.fr/activities/smos/data/l3

References

Adler, R. et al., (2016). Global Precipitation Climatology Project (GPCP) Climate Data Record (CDR), Version 2.3 (Monthly). National Centers for Environmental Information, doi:10.7289/V56971M6

Bates, N.R., R.J. Johnson (2020). Acceleration of ocean warming, salinification, deoxygenation and acidification in the surface subtropical North Atlantic Ocean. Commun Earth Environ 1, 33. https://doi.org/10.1038/s43247-020-00030-5

Blanke, B., and S. Raynaud (1997). Kinematics of the Pacific Equatorial Undercurrent: An Eulerian and Lagrangian Approach from GCM Results, J. Phys. Oceanogr., 27(6), 1038– 1053

Blanke, B., M. Arhan, G. Madec and S. Roche (1999). Warm water paths in the equatorial Atlantic as diagnosed with a general circulation model, J. Phys. Oceanogr., 29(11), 2753– 2768

Brodeau, L., B. Barnier, A.-M. Treguier, T. Penduff, and S. Gulev (2010). An era40- ´
based atmospheric forcing for global ocean circulation models. Ocean Modelling, 31 (3-4), 88–104.

Buckley, M.W., and J. Marshall (2016). Observations, inferences, and mechanisms of the Atlantic meridional overturning circulation: A review. Rev. Geophys. 54: 5–63. doi:10.1002/2015RG000493

Camara, I., N. Kolodziejczyk, J. Mignot, A. Lazar, and A.T. Gaye (2015). On the seasonal variations of salinity of the tropical Atlantic mixed layer, J. Geophys. Res. Oceans, 120, 4441–4462

Cessi, P. (2019). The global overturning circulation. Annu. Rev. Mar.Sci.,11, 249–270, doi:10.1146/annurev-marine-010318-095241

Claret M., R. Rodríguez and J.L. Pelegrí (2012). Salinity intrusion and convective mixing in the Atlantic equatorial undercurrent. Scientia Marina, 76(S1), 117–129, doi: 10.3989/scimar.03611.19B

Christian, J.R. and R. Murtugudde (2003). Tropical Atlantic variability in a coupled physical-biogeochemical ocean model. Deep Sea Research II, 50, 2947-2969.

Da-Allada, C.Y., F. Gaillard and N. Kolodziejczyk (2015). Mixed-layer salinity budget in the tropical Indian Ocean: seasonal cycle based only on observations. Ocean Dynamics 65, 845–857, doi.:10.1007/s10236-015-0837-7

Du, Y., Y. Zhang and J. Shi (2019). Relationship between sea surface salinity and ocean circulation and climate change. Science China Earth Sciences, Volume 62, Issue 5: 771-782

Durack, P. J., S.E. Wijffels and R.J. Matear (2012). Ocean salinities reveal strong global water cycle intensification during 1950 to 2000. Science, 336:455-458

Forget, G., J.M. Campin, P. Heimbach, C. N. Hill, R. M. Ponte and C. Wunsch (2015). ECCO version 4: an integrated framework for non-linear inverse modeling and global ocean state estimation. Geoscientific Model Development, 8, 3071-3104, doi:10.5194/gmd-8-3071-2015

Fukumori, I., O. Wang, I. Fenty, G. Forget, P. Heimbach, and R.M. Ponte (2017). ECCO Version 4 Release 3, http://hdl.handle.net/1721.1/110380, doi:1721.1/110380

Gao, S., T. Qu and X. Nie (2014). Mixed layer salinity budget in the tropical Pacific Ocean estimated by a global GCM, J. Geophys. Res. Oceans, 119, 8255–8270

Garzoli, S., and R. Matano (2011). The South Atlantic and the Atlantic Meridional Overturning Circulation. Deep Sea Research Part II: Topical Studies in Oceanography. 58. 1837-1847, doi:10.1016/j.dsr2.2010.10.063

Gaspar, P., Y. Grégoris and J.M. Lefevre (1990). A simple eddy kinetic energy model for simulations of the oceanic vertical mixing: tests at station papa and long-term upper ocean study site. Journal of Geophysical Research,95, 16,179–16,193

Gent, P. and J. Mcwilliams (1990). Isopycnal mixing in ocean circulation models, J. Phys. Oceanography., 20, 150–155

Gouriou, Y., and G. Reverdin (1992). Isopycnal and diapycnal circulation of the upper equatorial ocean in 1983-1984. J. Geophys. Res., 97: 3543-3572

Hanawa, K., and L.D. Talley (2001). Mode Waters. In Ocean Circulation and Climate, de. G. Siedler, J. Church and J. Gould, International Geophysical Series, Academy Press, New York, pp. 373-386

Hasson, A., T. Delcroix, and J. Boutin (2013). Formation and variability of the South Pacific Sea Surface Salinity maximum in recent decades. Journal of Geophysical Research-Oceans, 118(10), 5109–5116, doi:10.1002/jgrc.20367

Kara, A.B., P.A. Rochford and H.E. Hurlburt (2000). An optimal definition for ocean mixed layer depth, J. Geophys. Res., 105, 16,803 – 16,821, 2000a

Katsura, S., E. Oka, B. Qiu, and N. Schneider (2013). Formation and Subduction of North Pacific Tropical Water and Their Interannual Variability. J. Phys. Oceanogr., 43, 2400–2415, doi:10.1175/JPO-D-13-031.1.

Kim, S.B., T. Lee and I. Fukumori (2004). The 1997–1999 abrupt change of the upper ocean temperature in the north-central Pacific, Geophys. Res. Lett., 31, L22304, doi:10.1029/2004GL021142

Kim, S.B., I. Fukumori and T. Lee (2006). The closure of the ocean mixed layer temperature budget using level-coordinate model fields, J. Atmos. Oceanic Technol., 23, 840–853.

Köhler, J., N. Serra, F.O. Bryan, B.K. Johnson and D. Stammer (2018). Mechanisms of mixed-layer salinity seasonal variability in the Indian Ocean. Journal of Geophysical Research: Oceans, 123, 466–496. https://doi.org/ 10.1002/2017JC013640

Kubokawa, A. (1999). Ventilated thermocline strongly affected by a deep mixed layer: A theory for subtropical countercurrent, J. Phys. Oceanogr., 29, 1314–1333, doi:10.1175/1520-0485(1999)029<1314:VTSABA>2.0.CO;2

Le Vine, D.M., G.S. Lagerloef and S.E. Torrusio (2010). Aquarius and remote sensing of sea surface salinity from space. Proceedings of the IEEE, 98(5), pp.688-703.

Li, G., Y. Zhang, J. Xiao et al. (2019). Examining the salinity change in the upper Pacific Ocean during the Argo period. Clim Dyn 53, 6055–6074 , doi:0.1007/s00382-019-04912-z

Lukas, R. and E. Lindstrom (1991). The mixed layer of the western equatorial Pacific Ocean, J. Geophys. Res., 96(suppl), 3343–3357

Lumpkin, R., and K. Speer (2007). Global Ocean Meridional Overturning. J. Phys. Oceanogr., 37, 2550–2562, https://doi.org/10.1175/JPO3130.1

Madec, G. (2008). NEMO Ocean Engine, p. 300, Inst. Pierre-Simon Laplace, Paris, France.

Marshall J. C., A.J.G. Nurser and R.G. Williams (1993). Inferring the subduction rate and period over the North Atlantic. Journal of Physical Oceanography 23: 1315-1329

Marshall, J., A. Adcroft, C. Hill, L. Perelman and C. Heisey (1997). A finite-volume, incompressible Navier Stokes model for studies of the ocean on parallel computers, J. Geophys. Res., 102, 5753–5766

Metcalf, W. G., A. D. Voorhis, M. C. Stalcup (1962). The Atlantic Equatorial Undercurrent. J. Geophys. Res. 67: 2499-2508.

Piecuch, C. G., (2017). A note on evaluating budgets in ECCO Version 4 Release 3. (Available at ftp://ecco.jpl.nasa.gov/Version4/Release3/doc/evaluating_budgets_in_eccov4r3.pdf.)

Piola, A. and A. Gordon (1989). Intermediate waters in the southwest South Atlantic. Deep Sea Research Part A. Oceanographic Research Papers. 36. 1-16. 10.1016/0198-0149(89)90015-0.

Qiu, B., and R.X. Huang (1995). Ventilation of the North Atlantic and North Pacific: Subduction versus obduction. J. Phys. Oceanogr., 25, 2374–2390

Qu, T., S. Gao and I. Fukumori (2011). What governs the North Atlantic salinity maximum in a global GCM?, Geophys. Res. Lett., 38, L07602

Qu, T., S. Gao and I. Fukumori (2013). Formation of salinity maximum water and its contribution to the overturning circulation in the North Atlantic as revealed by a global general circulation model, J. Geophys. Res. Oceans,118, 1982–1994

Rodrigues, R.R., L.M. Rothstein and M. Wimbush (2006). Seasonal Variability of the South Equatorial Current Bifurcation in the Atlantic Ocean: A Numerical Study, J. Phys. Oceanography, 37 (1), 16–30, doi:10.1175/JPO2983.1

Roemmich, D. and J. Gilson (2009). The 2004-2008 mean and annual cycle of temperature, salinity, and steric height in the global ocean from the Argo Program. Progress in Oceanography, 82, 81-100, doi:10.17882/42182

Salisbury J. E. And B.F. Jonsson (2018). Rapid warming and salinity changes in the Gulf of Maine alter surface ocean carbonate parameters and hide ocean acidification. Biogeochemistry, 141, 401-418, doi:10.1007/s10533-018-0505-3

Schmitt, R.W. (2008). Salinity and the global water cycle. Oceanography 21(1):12–19, doi:10.5670/oceanog.2008.63

Schmitt, R.W. and A. Blair (2015). A river of salt. Oceanography, 28(1), pp.40-45.

Sprintall, J., and M. Tomczak (1992). Evidence of the barrier layer in the surface layer of the tropics, J. Geophys. Res., 97, 7305–7316

Thompson, P. R., C.G. Piecuch, M.A. Merrifield, J.P. McCreary, and E. Firing (2016). Forcing of recent decadal variability in the Equatorial and North Indian Ocean, J. Geophys. Res. Oceans, 121, 6762–6778, doi:10.1002/2016JC012132

Voituriez, B., and A. Herbland (1979). The use of the salinity maximum of the equatorial undercurrent for estimating nutrient enrichment and primary production in the Gulf of Guinea, Deep-sea Res., 24,

Wang, C. (2005). Subthermocline tropical cells and equatorial subsurface currents. Deep-Sea Res. I 52: 123-135

Wang, Y., Y. Li and C. Wei (2020). Subtropical sea surface salinity maxima in the South Indian Ocean. J. Ocean. Limnol. 38, 16–29, doi:10.1007/s00343-019-8251-5

Williams, R.G. (1991). The role of the mixed layer in setting the potential vorticity of the main thermocline. J. Phys. Oceanogr., 21, 1803–1814

Woods, J.D. (1985). The physics of thermocline ventilation. Coupled Ocean-Atmosphere Models, J. C. J. Nihoul, Ed., Elsevier Oceanography Series, Elsevier Science Publishers,543–590

Yu, L. (2007). Global variations in oceanic evaporation (1958–2005): The Role of the changing wind speed, J. Clim., 20, 5376–5390, doi:10.1175/2007JCLI1714.1

Yu, L. (2011). A global relationship between the ocean water cycle and near surface salinity, J. Geophys. Res., 116, C10025

Highlights

- Maximum salinity region has a mixed layer salinity modulated by an excess of evaporation over precipitation and entrainment.
- Maximum evaporation minus precipitation region is controlled by ekman transport of low salinity waters from near-equatorial regions.
- Maximum salinity waters spread northward into North and South Brazil Currents modulated by seasonal migration of South Equatorial Current bifurcation region.
- A subducted salt river (2.6 Sv) flows northward along the North Brazil Current and retroflects north of the equator as part of the Equatorial Undercurrent.

Declaration of Interests

☐ The authors declare that they have no known competing financial interests or personal relationships that could have appeared to influence the work reported in this paper.

☐The authors declare the following financial interests/personal relationships which may be considered as potential competing interests:

none